Thermal conductivity of giant mono- to few-layered CVD graphene supported on an organic substrate

Jing Liu,[a] Tianyu Wang,[a] Shen Xu,[a] Pengyu Yuan,[a] Xu Xu[b] and Xinwei Wang*[a,c]

The thermal conductivity (k) of supported graphene is a critical property that reflects the graphene–substrate interaction, graphene structure quality, and is needed for thermal design of a graphene device. Yet the related k measurement has never been a trivial work and very few studies are reported to date, only at the μm level. In this work, for the first time, the k of giant chemical vapor decomposition (CVD) graphene supported on poly(methyl methacrylate) (PMMA) is characterized using our transient electro-thermal technique based on a differential concept. Our graphene size is ~mm, far above the samples studied in the past. This giant graphene measurement eliminates the thermal contact resistance problems and edge phonon scattering encountered in μm-scale graphene k measurement. Such mm-scale measurement is critical for device/system-level thermal design since it reflects the effect of abundant grains in graphene. The k of 1.33-layered, 1.53-layered, 2.74-layered and 5.2-layered supported graphene is measured as 365 W m^{-1} K^{-1}, 359 W m^{-1} K^{-1}, 273 W m^{-1} K^{-1} and 33.5 W m^{-1} K^{-1}, respectively. These values are significantly lower than the k of supported graphene on SiO_2, and are about one order of magnitude lower than the k of suspended graphene. We speculate that the abundant C atoms in the PMMA promote more ready energy and momentum exchange with the supported graphene, and give rise to more phonon scattering than the SiO_2 substrate. This leads to a lower k of CVD graphene on PMMA than that on SiO_2. We attribute the existence of disorder in the sp^2 domain, graphene oxide (GO) and stratification in the 5.2-layered graphene to its more k reduction. The Raman linewidth (G peak) of the 5.2-layered graphene is also twice larger than that of the other three kinds of graphene, indicating the much more phonon scattering and shorter phonon lifetime in it. Also the electrical conductivity of the 5.2-layered graphene is about one-fifth of that for the other three. This further confirms the poor graphene quality of sample 4S, explaining its much lower k.

1. Introduction

Since graphene was first discovered in 2004,[1] it has drawn enormous attention for its unique properties. These properties, including very high thermal conductivity (k),[2,3] super electronic mobility,[4] rich optical properties,[5] as well as remarkable mechanical strength,[6] have led to many promising applications. Examples of such applications include microelectronics,[7] photovoltaic devices, touchable screens, optical frequency converters[5] and so on. The k of graphene is an important factor in its potential applications with the increasing intense heat density in nanoelectronics. The maximum k of the suspended single-layered graphene (SLG) has been reported to be ~5300 W m^{-1} K^{-1} at room temperature (RT). Balandin *et al.* used confocal micro-Raman spectroscopy to obtain the dependence of the G peak with a frequency of μm size SLG on the excitation laser power. With an independently measured G peak temperature coefficient, the k of suspended SLG is extracted.[2] Isotopically pure graphene was measured by Chen *et al.* through a non-contact optothermal Raman technique. The k was found to be higher than ~4000 W m^{-1} K^{-1} when temperature (T) is ~320 K.[8] Numerical studies showed that the lattice thermal conductivity of few-layered graphene (FLG) decreases with increasing layer number due to the fact that interlayer coupling breaks the graphene selection rule.[9] Experiments also proved that the k of suspended graphene decreases with increasing layer number and finally saturates at the level of bulk graphite.[10] When a micro-size suspended graphene is under the thermal conductivity test, the thermal contact resistance between the micro-

[a]2010 Black Engineering Building, Department of Mechanical Engineering, Iowa State University, Ames, IA 50011, USA. E-mail: xwang3@iastate.edu; Tel: +1 515 2948023
[b]School of Metrological and Measurement Engineering, China Jiliang University, Hangzhou 310018, Zhejiang Province, P. R. China
[c]School of Environmental and Municipal Engineering, Qingdao Technological University, Qingdao 266033, Shandong Province, P. R. China

size graphene and the supporting ends is still not well known and could affect the results to a significant extent. Also, the thermal resistance of the measured suspended graphene is not very large due to its µm size. The phonon scattering due to the edge boundary could be strong for µm size graphene. Last but not least, rare grains exist in µm size graphene, which results in a weak grain-boundary phonon scattering effect. As a result, the measured results reflect little effect of grains within a graphene sheet.

Even though suspended graphene shows an extremely high k at RT, the k of supported graphene reduces to hundreds W m^{-1} K^{-1}. Seol et $al.$ measured the $k \sim T$ relationship for monolayer graphene exfoliated on amorphous SiO$_2$ through a bridge method. k was determined to be ~600 W m^{-1} K^{-1} at RT when the sample size is 1.5 to 3.2 µm in width and 9.5 to 12.5 µm in length. This value is still considerably high even though it is only one-ninth of that of suspended graphene. The authors found that the flexural phonon mode (ZA) makes a large contribution to k in suspended graphene by using the Boltzmann transport equation (BTE) method. The contribution percentage could be 77% for suspended graphene at 300 K. They attribute the k reduction of supported graphene to phonon leakage across the graphene–SiO$_2$ interface in supported graphene. The BTE calculations reveal significant reduction of ZA contribution to k of supported graphene.[11] Chen et $al.$ used non-equilibrium molecular dynamics (NEMD) simulation to study the thermal transport in the SiO$_2$-supported graphene. The k of SiO$_2$-supported SLG is predicted to be ~600 W m^{-1} K^{-1}, and the k of supported FLG is found to increase with the thickness of graphene by experiment.[12,13] It is also found that different coupling strengths caused by different choices of substrates are critical for supported graphene thermal transport.[13,14] A strong graphene–substrate coupling strength (χ) significantly increases the ZA mode scattering in graphene, which leads to more reduction of k when χ increases.[9,12] However, some other researchers found that a higher graphene–substrate coupling strength increases the k by using the spectral energy density (SED) analysis.[13] Different simulation methods cause the discrepancy. Experiments are needed to further explore the relationship between the k of supported graphene and graphene–substrate coupling strength.

So far, the thermal conductivity measurement for supported graphene has been at the micrometer scale. No work has been reported on the k measurement of large-area CVD graphene. The same scenario also applies to suspended graphene k measurements in terms of the size effect. The k of suspended SLG is found to increase with length when the length of the suspended graphene is at the level of several µm.[9,15] The size of measured suspended graphene is several µm in a former research,[2,15,16] so the size effect plays a significant role in thermal transport of graphene.[17] For microscopic FLG, the phonon scattering contribution to k is limited by the size of the flake and defects rather than the Umklapp scattering.[10] The edge-phonon scattering usually causes great reduction in k. Furthermore, graphene is a soft conductive material which has important applications in flexible electronic devices and

sensors. No work has been reported on k measurement of large-area graphene on soft substrates, yet such knowledge is critical for performing device design and optimization.

Since graphene is extremely thin (~nm), it is difficult to obtain a giant suspended graphene of mm size, not mentioning the k measurement at such a level. Usually a supported graphene is chosen for study purpose. Even for a giant size supported graphene, the significant effect of a substrate on the overall k could overshadow the effect of graphene's thermal conductance. As a result, it becomes extremely difficult to determine graphene's k. To overcome this extreme difficulty, we use an extremely thin poly(methyl methacrylate) (PMMA) (~500 nm) substrate to support the graphene under measurement. Since PMMA has a very low k (0.21 W m^{-1} K^{-1}), the overall effect of PMMA on heat conduction is comparable to that of graphene. This makes it possible to measure the k of graphene with high accuracy. So far, most of the work about the k measurement of graphene has been conducted through Raman spectroscopy, which means that only the k of micro-size graphene could be measured.[2,8,10] In this work, for the first time, the k of giant size supported graphene on PMMA is measured by a differential technology. The sample size is around 1 to 2 mm in width (W) and to 2 to 4 mm in length (L). This type of size significantly suppresses the effect of edge boundary scattering of phonons and the thermal contact resistance effect at the electrode ends. Silver paste is used to give a sound contact (thermal, mechanical and electrical) between the sample and the electrode ends due to the large size of the sample. Under this situation, the thermal contact resistance becomes very small and negligible. The radiation effect exists while measuring the k of the supported graphene. By measuring samples with different lengths, the radiation effect on k is precisely subtracted. Here, we report the k measurement of 1- to ~6-layered CVD graphene supported by PMMA. The k of supported graphene is found at the level of ~360 W m^{-1} K^{-1} at RT. It does not show evident relationship with graphene layer numbers.

2. Sample preparation and characterization

Graphene supported by PMMA tested in this experiment is obtained from Advanced Chemical Supplier Company. Totally four kinds of graphene samples supported by PMMA are tested. They are single-layered graphene (1S), two-layered graphene (2S), three- to five-layered graphene (3S) and six- to eight-layered graphene (4S). The layer numbers of graphene are offered in the technical data of the samples. We also conducted a separate measurement of the layer numbers after the samples were received. In this work, the sample index is used as this: '2S8' means the eighth tested sample of 2S. The preparation method for the supported graphene is described as follows. The graphene is grown on a copper (Cu) foil through a controlled chamber pressure CVD (CP-CVD) system. A clean Cu foil was first annealed at 1077 °C with a H$_2$ flow rate of 500

sccm. Then the H_2 flow rate and the chamber pressure were adjusted to 70 sccm and 108 Torr, respectively. The graphene started to grow by introducing 0.15 sccm CH_4 into the chamber.[18] After the reaction, the copper was etched off after PMMA was coated on the graphene. Finally, graphene supported by PMMA was transferred onto a polymer substrate.

Fig. 1(a) shows the steps to cut the sample from the originally purchased graphene into a desired sample size. First, the supported graphene is released into distilled water and then picked up by a filter paper. The supported graphene is then cut into desired sizes with scissors. After obtaining a desired experimental sample, the supported graphene is transferred to the electrode substrate, which is shown in Fig. 1(b). This is used for measurement of k by the transient electro-thermal (TET) technique.[19,20] The morphology of sample 2S8 was also investigated using a scanning electron microscope (SEM). The SEM pictures are shown in Fig. 1(c) and (d), with clear grains visible at the level of tens to hundreds of μm. Even though the layer numbers are given in the technical data sheet of these samples, the quality and the layer number of the samples need to be examined and verified. It is necessary to know whether the graphene distributes uniformly on PMMA for the TET measurement. So the layer number of the graphene is characterized by a confocal Raman system (Voyage, B&W Tek, Inc. and Olympus BX51).

Taking sample 2S3 as an example, a 532 nm Raman laser of ~0.77 mW is focused on the graphene with a 50× objective. The integration time varies from 8 to 10 s for different spots on the graphene. Spectra of sample 2S3 are shown in Fig. 2. It can be found that the D band (~1340 cm^{-1}) for 2S3 is absent from the spectrum, meaning that 2S3 has rare D-band related defects. Peaks at around 1586 cm^{-1} (G band) and 2690 cm^{-1} (2D band) are observed. The number of layers is obtained by evaluating I_G/I_{2D}.[21] Totally 15 random spots on 2S3 are tested. Fig. 2 also indicates the layer number determined using the Raman spectrum for each spot. The area percentage of single-layered, two-layered and three-layered graphene is 53.3%, 40.0% and 6.7% respectively. The overall average number of layers is calculated to be 1.53 for sample 2S. Using the same method, the average layer number is determined to be 1.33 and 2.74 for samples 1S and 3S, respectively.

The representative Raman spectra of 4S are shown in Fig. 8 and will be discussed in detail later. Three pronounced peaks at about 1346, 1589 and 2681 cm^{-1} are observed, corresponding to the D band, G band and 2D band, respectively. The D band originates from the defects and the disorder structure in the sp^2 domains of graphene.[22] No D band is observed in 1S, 2S and 3S, meaning they are defect-free graphene samples. Besides, some G bands of 4S (e.g., spectra a, b, c and d in Fig. 8) show the characteristic of peaks that contain two peaks.
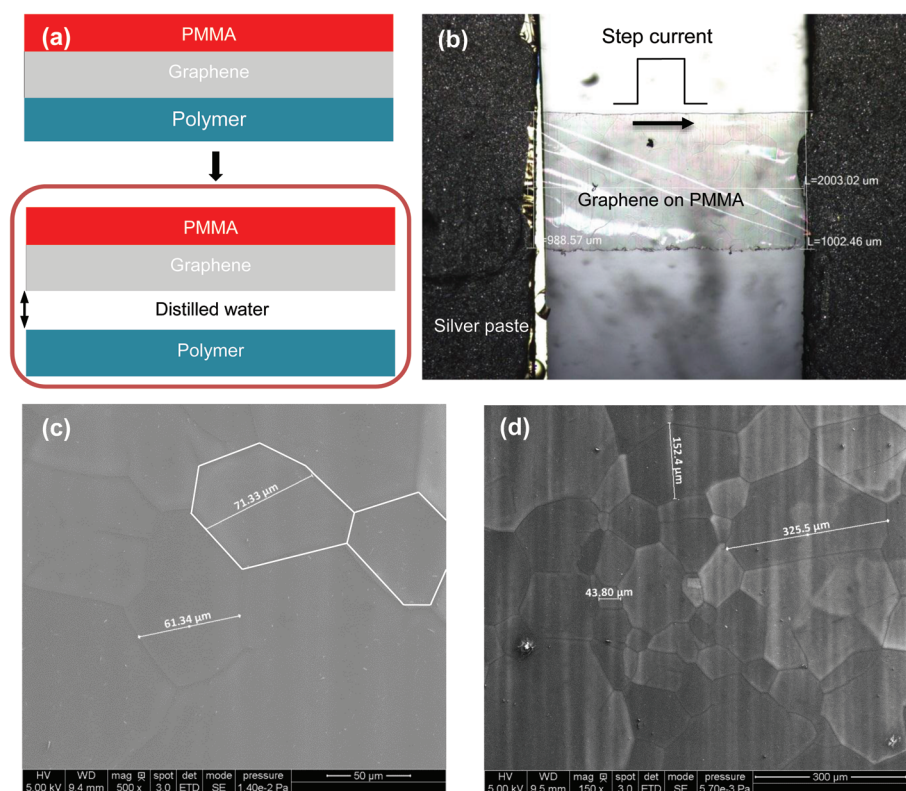

Fig. 1 (a) Steps to obtain the desired size sample from the as-purchased graphene (not to scale). (b) Sample 2S3 (under microscope) connected between two electrodes. (c) and (d) SEM images of sample 2S8. Clear grains can be seen with a characteristic size of tens to hundreds of μm. The graphene thickness has a non-uniform distribution on the PMMA according to Raman spectroscopy. Grains are studied using Raman spectroscopy to determine the layer number. In (c), the white lines depict representative grains of graphene.
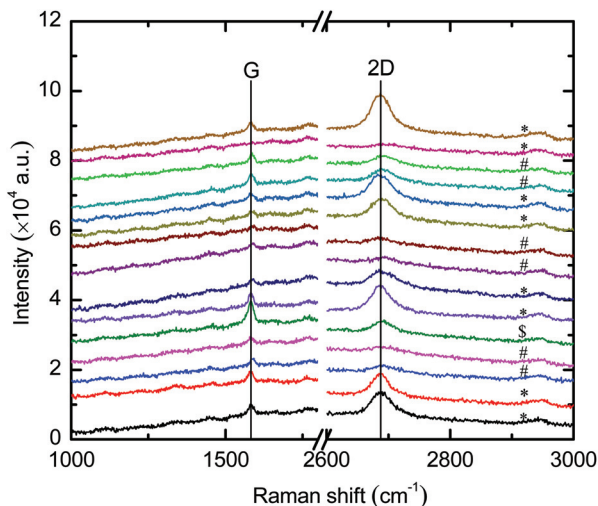
Fig. 2 Raman spectra of sample 2S3. Clear G band and 2D band are observed. '*', '#' and '$' above each Raman spectrum indicate single-layered, double-layered and three-layered graphene, respectively. The area percentage of single-layered, double-layered and three-layered graphene are 53.3%, 40.0% and 6.7%, respectively. The overall average layer number is calculated to be 1.53 for sample 2S.

This may arise from the stratification among multiple-layered graphene. Under this situation, it is not reasonable to determine the graphene layer number using the Raman method. Here, we determine the graphene layer number of sample 4S by measuring its optical transmittance. A laser beam (532 nm) with known incident energy is irradiated on the sample surface, while an energy power meter is used to measure the transmitted energy at the same time. The transmittance is determined to be 81.48%. The refractive indexes of air, PMMA and graphene are 1, 1.49 and 2.4, respectively. The extinction coefficient of graphene is ~1.3.[23] These values are used in graphene layer number determination. The average graphene layer number is calculated according to the transmittance coefficient by using the transfer matrix method (TMM).[24] The layer number of sample 4S is determined to be 5.2. This value will be used when calculating the k of graphene. The thickness of PMMA is also needed to calculate the k of graphene by subtracting the effect of PMMA. The mass of PMMA (m) is measured by thermogravimetric analysis (TGA). With the knowledge of surface area (A) and density (ρ) of the PMMA, the thickness of PMMA (δ_p) is determined to be $\delta_p = m/(A \cdot \rho)$. The density of PMMA is 1180 kg m^{-3} in this equation.[25] The thicknesses of PMMA and graphene layer numbers for the four samples are summarized in Table 1.

3. Abnormal temperature coefficient of resistance for PMMA-supported graphene

The TET technique is used for determining thermal properties. During the measurement, a step current is fed through

Table 1 PMMA thickness, average layer number, intercept, slope of linear fit and emissivity for 1S, 2S, 3S and 4S

Sample	1S	2S	3S	4S
PMMA thickness (nm)	790.06	632.63	825.65	630.95
Average layer number	1.33	1.53	2.74	5.20
Intercept	2.46×10^{-7}	2.46×10^{-7}	2.94×10^{-7}	2.23×10^{-7}
Slope	0.112	0.103	0.0992	0.197
Emissivity	0.128	0.0943	0.119	0.181

the sample to cause Joule heating. The Joule heating leads to a temperature rise in the sample, which is recorded by measuring the voltage over the sample. Generally, the resistance of graphene decreases with increased temperature.[26] However, we find that upon heating and temperature rise, the resistance of the graphene supported by PMMA goes up instead of decreasing like many reported graphene samples (detailed in section 4) at RT. This section is designed to study the temperature coefficient of the resistance (TCR) of our graphene samples before we elaborate on the thermal characterization.

For TCR measurement, due to the fragile nature of the sample under low temperatures, the supported graphene is placed on a glass side and silver paste is used to connect the sample with two electrodes. Then the sample is placed in a vacuum chamber of a cryogenic system (CCS-450, JANIS). A liquid nitrogen cold-trapped mechanical vacuum pump is used to make the vacuum level under 0.5 mTorr. This is intended to reduce the water content impact in the chamber at low temperatures. The resistance of the sample is detected by using a $6\frac{1}{2}$ digital multi-meter (Agilent 34401A). Since the resistance of different samples varies a lot, a normalized resistance (ratio of the resistance over that at RT) for samples with different layer numbers are presented in Fig. 3(a). The inset shows a close up of the normalized resistance between 100 K and 220 K. It can be seen that at around RT, the resistance decreases a little bit when temperature decreases, giving a positive TCR. After reaching a minimum value, resistances of 1S and 2S_1 begin to rise as temperature decreases. However, the resistances of 3S and 4S increase a little bit and then drop again with temperature decreasing. The maximum resistance decrease is 0.071% among the five $R \sim T$ tests. The electrical resistance of graphene supported on flexible substrates under tensile strain has been studied by Hinnefeld *et al.* They found that the tensile strain in the supported graphene could cause rips in the graphene, and these rips are reversible. These rips cause the supported graphene resistance to increase significantly.[27]

Combined effects including positive thermal expansion of the PMMA (β_p), negative thermal expansion coefficient of graphene (β_g) and intrinsic resistance change of relaxed graphene against temperature (β) determine the observed $R \sim T$ jointly. As shown in Fig. 3(b), PMMA and graphene have different thermal expansion coefficients (TEC).[28,29] When temperature
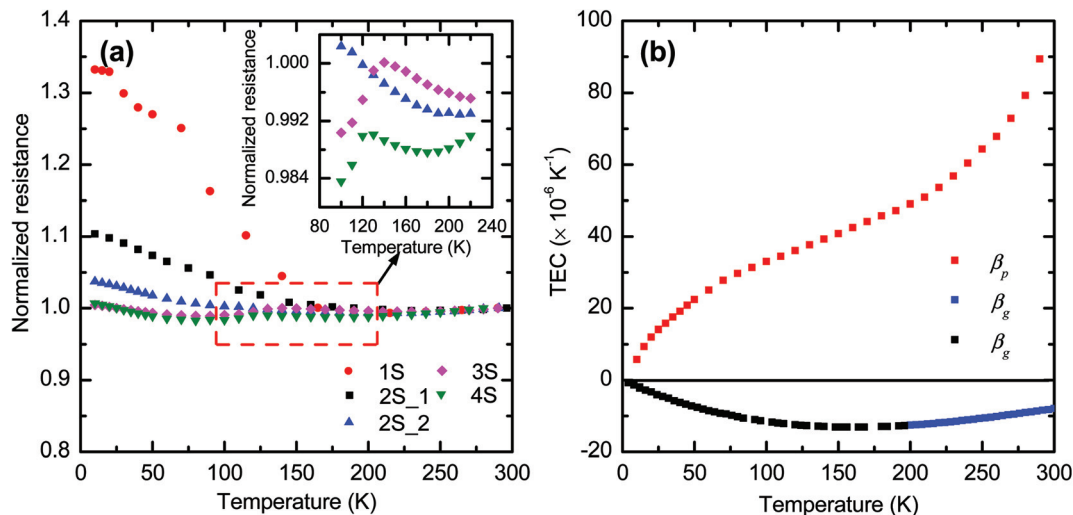
Fig. 3 (a) Normalized resistance for 1S, 2S, 3S and 4S, respectively. The RT resistances for 1S, 2S_1, 2S_2, 3S and 4S are 0.614 kΩ, 2.494 kΩ, 2.587 kΩ, 1.782 kΩ and 3.422 kΩ, respectively. The inset shows a close up of the normalized resistance between 100 K and 220 K. (b) Thermal expansion coefficient of PMMA (from experiment) and suspended SLG.[28,29] Data shown in blue square are obtained by the experiment fitting. The data shown in black square are the estimated values.

changes, PMMA and graphene will intend to have different thermal expansions. Since they are tightly held together by the van der Waals force between them, strain and stress will be built up in graphene. This strain/stress will change the resistance of graphene accordingly. Therefore, the overall TCR of graphene could be described as the following equation: $dR/dT = -\beta + (\beta_p - \beta_g)\gamma$, among which γ is a positive constant coefficient. β_p increases with increasing temperature and remains positive when temperature is above 0 K.[28] β_g is strongly dependent on the temperature but remains negative when the temperature is under RT according to experiments and theoretical calculations.[29–31] When the temperature is high, the TEC of PMMA is very large, making the overall TCR positive. When the temperature is low, the TEC of PMMA and graphene becomes small compared with the effect of β, making the TCR negative as shown in Fig. 3(a). However, the sudden increase of TCR for sample 1S when the temperature is reduced to around 150 K indicates that part or most of the graphene separates from PMMA. Under such a scenario, the TCR is determined largely by β since the stress in graphene due to thermal expansion mismatch is released by the separation. In our experiment, since the TET measurement is conducted at RT, the resistance of the sample will increase upon Joule heating as will be shown and discussed in the next section.

4. Thermal characterization of giant supported graphene

4.1. Details of TET measurement of the thermal diffusivity

Supported graphene samples with different layers and lengths are used to conduct the TET test. As shown in Fig. 4(a), the

supported graphene on PMMA is suspended between two gold-coated silicon electrodes. Silver paste is used to secure the contact between graphene and the electrodes. And then the sample is placed in an iridium coating machine (EMS 150T S) which helps maintain the high vacuum (below 0.6 mTorr) to conduct the TET test at RT. This is for eliminating the heat convection effect in the measurements. During the thermal characterization, a step current provided by a current source (Keithley 6221) is fed to the sample to induce a temperature rise in the sample. The change in the temperature leads to the change in resistance and thus the voltage. An oscilloscope (Tektronix DPO3052) is used to monitor and capture the voltage evolution of graphene. A normalized temperature change curve derived from voltage evolution is used for fitting and determining the effective thermal diffusivity (α_{eff}). The experimental normalized temperature change can be calculated as $\Delta T^* = (V - V_0)/(V_1 - V_0)$, where V_0 and V_1 are the initial and final voltages over the sample. The TET technique has been proven rigorously to be a quick and effective method to measure the thermal diffusivity of various conductive and non-conductive micro/nanoscale samples. More details could be found in ref. 19 and 32.

As seen from Fig. 4(a), the heat conduction along the sample can be treated as one-dimensional. Since the gold-coated silicon is much larger than the sample dimension, the temperature of the electrodes can be assumed unchanged even though a small current goes through it. The boundary conditions for this heat transport can be described as $\Delta T(x = 0) = 0$, where $\Delta T = T - T_0$ (T_0: room temperature). The governing equation is

$$\frac{\partial(\rho c_p T)}{\partial t} = k\frac{\partial^2 T}{\partial^2 x} + \dot{q}, \tag{1}$$
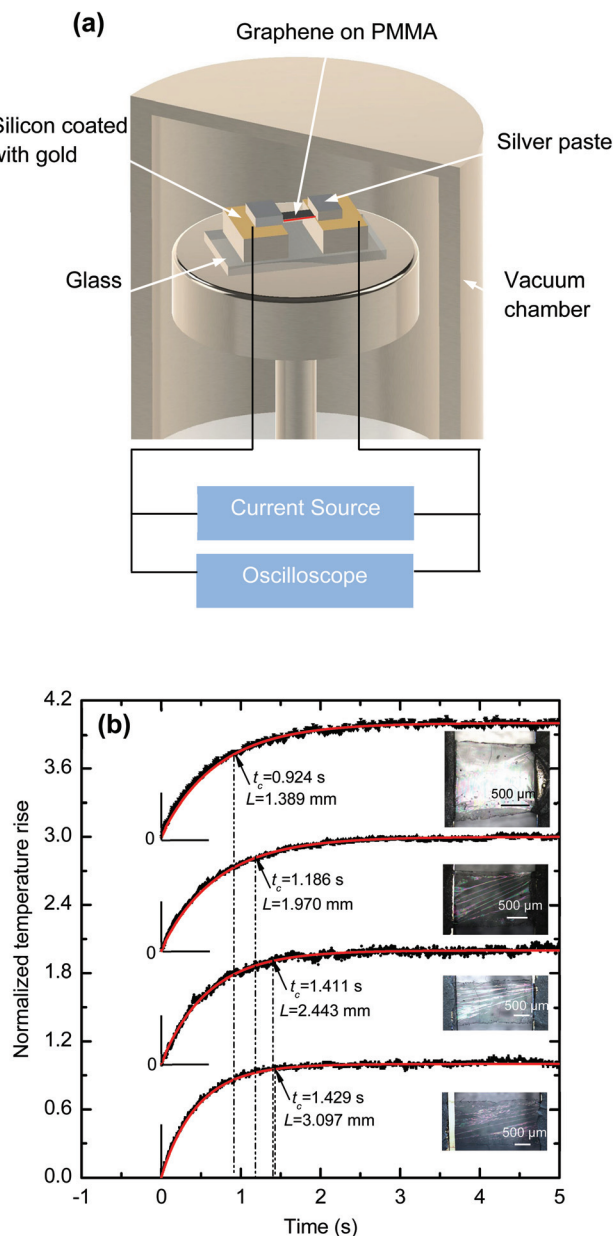
Fig. 4 (a) Schematic setup for the TET measurement (not to scale). (b) Normalized temperature rise evolution and TET fitting results for sample 1S with different lengths. The results of different experiments are shifted in the vertical direction to enhance the view. The insets are the samples under a microscope. It can be seen that the characteristic time (t_c) increases with increasing sample length. The black dots are the original data, and the fitting curves are shown in red.

$$T* = \frac{96}{\pi^4} \sum_{m=1}^{\infty} \frac{1 - \exp[-(2m-1)^2 \pi^2 \alpha_{eff} t / L^2]}{(2m-1)^4}. \qquad (2)$$

From eqn (2), it can be seen that the normalized temperature rise is only dependent on $\alpha_{eff} t / L^2$. The thermal diffusivity could be directly determined by the characteristic point of the $T* \sim t$ curve. Details could be found in ref. 19. The characteristic point is obtained when $T*$ is 0.8665 according to eqn (2). The relationship of the thermal diffusivity and characteristic time (t_c) is $\alpha_{eff} = 0.2026 L^2 / t_c$ for quick analysis in addition to global data fitting. For global data fitting, different trial values of α_{eff} are applied in eqn (2) in a Matlab program and the $T*$ value is compared with the experimental results. The trial α value which gives the best fit of the experiment data is taken as the sample's α_{eff}.

One point needs to be explained here that some wrinkles could be observed on the sample in Fig. 1(b) and 4(b). The wrinkles are due to the stretching along the sample during sample preparation. They will degrade the contact among graphene flakes. This has been proved by the electrical resistance increase by the wrinkles. But this will not affect the heat transfer in the axial direction of the sample since the graphene will transfer the heat to the PMMA, which connects graphene flakes in a parallel way. The wrinkles will increase the thermal contact resistance between graphene flakes and the PMMA substrate at some locations. This kind of interface resistance has a negligible effect on the thickness-directed heat conduction which will be described in section 4.3. The size of the wrinkles is at the ~mm scale, which is much larger than the size of graphene flakes (~10–100 μm). Therefore, the macroscopic wrinkles have limited effects on the graphene flake structure and its intrinsic thermal conductivity.

4.2. Effect of radiation

In the TET measurement, the radiation could have strong effects on the measurement. The real thermal diffusivity (α_{real}) of the sample is obtained after taking out the radiation effect as:[19,33]

$$\alpha_{real} = \alpha_{eff} - 8\varepsilon k_B T^3 L^2 / (\pi^2 \delta \rho c_p). \qquad (3)$$

In the above equation, δ, ε and k_B are the thickness of PMMA, emissivity and Stefan–Boltzmann constant, respectively. Different samples with different lengths are used to conduct the TET experiments, which aims at eliminating the effect of radiation.

Fig. 4(b) shows the normalized temperature rise evolution ($T* \sim t$) and fitting results when the experiments are conducted at RT for sample 1S. Magnificent fitting is obtained. The insets are the samples under a microscope. It is clear that t_c increases with increasing sample length, which is consistent with our fitting results. According to eqn (3), we can see that α_{eff} and length square (L^2) have a linear relationship. The intercept at the y-axis of the $\alpha_{eff} \sim L^2$ relationship is the real thermal diffusivity of the sample. The $\alpha_{eff} \sim L^2$ linear fitting for four kinds of graphene samples are shown in Fig. 5. The linear fitting intercepts and slopes for four kinds of graphene

where ρ, c_p and k are the density, specific heat and thermal conductivity of the sample, respectively. $\dot{q}$ is the electrical heating power per unit volume with the form $I^2 R_s / AL$, where A and L are the cross-sectional area and length of the sample, respectively. I and R_s are the fed-in current and the resistance of the sample, respectively. The normalized temperature rise, which is defined as $T*(t) = [T(t) - T_0]/[T(t \to \infty) - T_0]$, is solved as
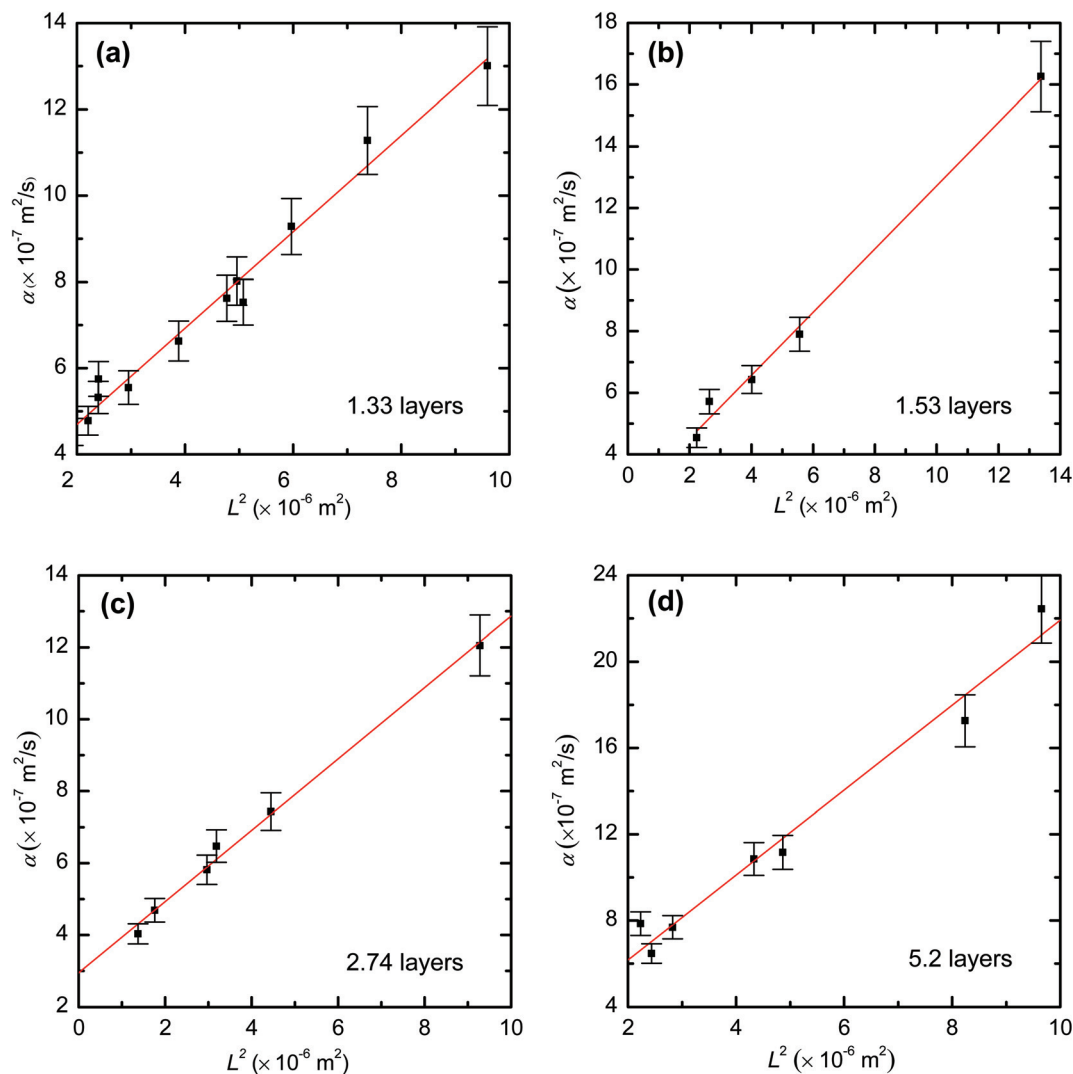
Fig. 5 Linear fit of $\alpha_{\text{eff}} - L^2$ for (a) 1.33-layered graphene; (b) 1.53-layered graphene; (c) 2.74-layered graphene; and (d) 5.2-layered graphene. The black dots are the original data, and the linear fitting lines are shown in red. The intercepts and slopes are listed in Table 1. The relative error of each measurement is calculated to be less than 7%. The error bars are shown in the figures.

samples are summarized in Table 1. Also, with the knowledge of fitting slope, PMMA thickness and temperature, the emissivity of the four kinds of graphene samples can also be determined when the slope is divided by $8k_{\text{B}}T^3/(\pi^2\delta\rho c_{\text{p}})$. The determined emissivity of four graphene samples is summarized in Table 1. The emissivity of the first three kinds of graphene samples is consistent with each other and close to ~0.1. Documents show that SLG absorbs ~2.3% fraction of incident photon energy over a wide wavelength range.[34,35] Besides, the opacity of the graphene is found to increase linearly with increasing graphene layers. The light absorbance could be ~11.8% for the five-layered graphene according to published research.[35] It is reasonable that the emissivity of the sample 4S is a little bit higher than the other three graphene samples. Furthermore, Dawlaty *et al.* measured the absorbance of a 6-layered graphene. They found that the absorbance varies from ~0.25 to ~0.035 when the wavelength varies from 100 μm

to 10 μm.[36] The discrepancy between our results and the documented values could be ascribed to different light absorbances at different wavelengths. Additionally, our measured emissivity is for all directions while in ref. 33, the absorbance is for the normal direction. The direction difference could also cause the discrepancy between our results and the documented values. Past work has shown that the emissivity of PMMA is ~2.6% at ~7 μm for a 250 μm-thick sample.[37] For our PMMA film with hundreds of nm thickness, the emissivity could be smaller since the absorption of PMMA is a volumetric effect. Therefore the PMMA will have a very small contribution to the measured emissivity.

4.3. Effect of cross-plane heat conduction

In our thermal characterization, the graphene layer is heated first by the electrical current, and then it transfers energy to the PMMA substrate. Since the graphene layer is ~nm thick,

and the PMMA substrate is several hundred times thicker, a natural question is: will the graphene and PMMA have thermal equilibrium in the cross-sectional direction? How does the heat conduction in the cross-section affect the measurement results? First of all, taking one supported graphene sample as an example, analysis is conducted for the effect of thermal contact resistance between graphene and PMMA. The picked sample 1S is 2 mm in length and 1.2 mm in width. When the k of PMMA is 0.21 W m^{-1} K^{-1} and the thickness of PMMA is 790 nm, the thermal resistance for PMMA conduction is ~5.02 × 10^6 K W^{-1}. The interfacial thermal conductance between graphene and PMMA obtained by Cai *et al.* is ~28 MW m^{-2}.[38] Their graphene supported on PMMA has been produced with the same method as our samples. So the interfacial thermal resistance for our samples can be estimated as 0.0419 K W^{-1}. This value is much smaller than the PMMA thermal resistance in the axial direction. Therefore, it is physically reasonable to conclude that the interfacial thermal resistance between graphene and PMMA in our sample has a negligible effect on the thermal transport in the axial direction.

In our experiment, the graphene is extremely thin (~nm) compared with the PMMA substrate (632 nm–830 nm). A natural question is: when graphene is heated up by the electrical current, whether it has sufficient time to conduct the heat to PMMA to reach thermal equilibrium in the cross-plane direction? For graphene, its thermal relaxation time (τ_g) can be estimated as $\tau_g \approx \delta_p R''_{tc} \rho c_p$, where R''_{tc}, ρ and c_p are thermal contact resistance, graphene density and heat capacity, respectively. For a SLG, when the graphene thickness, thermal contact resistance and volumetric heat capacity are taken as 0.335 nm, 1×10^{-9} m^2 K W^{-1} and 1.5×10^6 J m^{-1} K^{-1}, respectively, τ_g is estimated as 0.5 ns. For the heat conduction across the thickness direction of PMMA, its characteristic time can be estimated using this equation: $\tau_p = \delta_p{}^2/\alpha_p$, where α_p is the thermal diffusivity of PMMA. When the thickness of PMMA is 790 nm, and the thermal diffusivity of PMMA is 1.25×10^{-7} m^2 s^{-1}, the estimated cross-plane characteristic time for PMMA during TET measurement is 5 μs. Both characteristic times are much smaller than the characteristic time taken to reach the thermal steady state in the TET measurement, which is in the order of seconds as shown in Fig. 4(b). This means the temperature of graphene and PMMA at the axial same point have the same temperature during the transient thermal transport process.

Furthermore, a numerical study of this transient electro-thermal transport in the supported graphene is also conducted by using ANSYS to double check the situation. The dimensions of graphene are 1.54 mm in length and 0.335 nm in thickness, and the dimensions of PMMA are 1.54 mm in length and 790 nm in thickness. The k, c_p and ρ of graphene used in the simulation are 316 W m^{-1} K^{-1}, 709 J kg^{-1} K^{-1}, and 2210 kg m^{-3}, respectively. The k, c_p and ρ of PMMA used in the simulation are 0.21 W m^{-1} K^{-1}, 1466 J kg^{-1} K^{-1}, and 1180 kg m^{-3}, respectively. The initial temperature of the sample is 298.15 K. Boundary conditions for the sample are: the emissivity for the upper surface and the lower surface is 0.13, temperature of two ends is considered to remain at 298.15 K during Joule heating.

The heat generated in the sample is 0.0296 mW. The total simulation time is 5 s with a 0.01 s time-step interval. Fig. 6 shows the graphene temperature evolution with time and difference between the temperature of PMMA and graphene in the middle along the axial direction. It is seen the graphene has an overall temperature rise of ~5 °C. Meanwhile the temperature difference between PMMA and graphene is in the order of 10^{-5} °C. Therefore, the temperature of graphene and PMMA could be regarded the same during Joule heating.

5. Intrinsic thermal conductivity of graphene

After obtaining α, the effective thermal conductivity (k_{eff}) with the effects from PMMA and graphene can be determined as: $k_{eff} = \alpha(\rho c_p)_p$. Since the mass proportion of graphene in the composite is very small, the volumetric heat capacity of PMMA can be used for the whole sample with a high accuracy. Just as discussed in the graphene layer number determination part, the graphene distribution on the PMMA is not uniform. For example, there are single-layered, two-layered and three-layered graphene on PMMA for sample 2S. In this situation, the supported graphene can be seen as a composite filled with multiple fillers. The fillers are PMMA and the corresponding on-top graphene of different layers. The k of graphene (k_g) could be determined through the modified Nielsen Model to rule out the effect of PMMA. The modified Nielsen model is written as:[39]

$$\frac{k}{k_m} = \left[1 + \sum_{i=1}^{n} A_i \cdot B_i \cdot \Phi_i\right] \bigg/ \left[1 - \sum_{i=1}^{n} B_i \cdot \Psi_i \cdot \Phi_i\right], \quad (4)$$
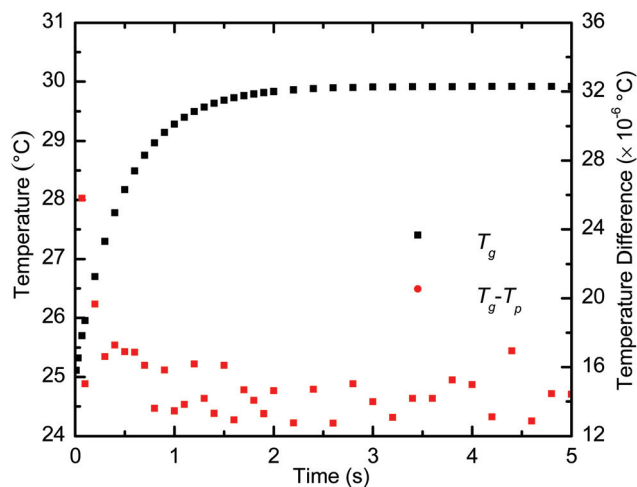

Fig. 6 Graphene temperature evolution with time and difference between the temperature of PMMA and graphene in the middle along the axial direction. It is seen that the graphene has an overall temperature rise of ~5 °C. Meanwhile the temperature difference between PMMA and graphene is in the order of 10^{-5} °C. It is reasonable to conclude that the temperature of PMMA and graphene are almost the same during the TET measurement.

$$B_i = \frac{k_i/k_{\mathrm{m}} - 1}{k_i/k_{\mathrm{m}} + A}, \tag{5}$$

$$\Psi_i \cong 1 + \frac{1 - \Phi_{mi}}{\Phi_{mi}^2} \cdot \Phi_i. \tag{6}$$

k and k_{m} are the thermal conductivity of the composite and base matrix. k_i represents the thermal conductivity of each filler. The subscript 'i' represents different fillers. Φ_i is the volume fraction of each filler. A_i and Φ_{mi} are the shape factor and maximum packing fraction. In this sample, the graphene fillers could be regarded as uniaxial oriented fibers, and the thermal conductivity measured in this experiment is that transverse to the fiber axial direction. Based on this condition, A_i and Φ_{mi} are chosen to be 0.5 and 0.82.[39] Ψ_i is a constant taking the orientation and the packing of the filler in the matrix into account.

k_i (each filler) is written as $k_i = (n\delta k_{\mathrm{g}} + \delta_{\mathrm{p}} k_{\mathrm{p}})/(n\delta + \delta_{\mathrm{p}})$. δ is the thickness of single layered-graphene, and it is taken as 0.335 nm, which is the interlayer spacing in graphite. n is the graphene layer number of each filler. Taking the sample 2S as an example, its k_{eff} is calculated to be 0.422 W m^{-1} K^{-1}. The filler 1 (single-layered graphene on PMMA) is chosen to be the base matrix, since it has the biggest volume fraction (0.533). The volume fraction of filler 2 (two-layered graphene on PMMA) and filler 3 (three-layered graphene on PMMA) is 0.4 and 0.067, respectively. By trying different values of k_{g}, k of the composite is determined according to eqn (4)–(6). When the k of the composite is equal to the measured k_{eff} of sample 2S, the corresponding value of k_{g} is taken to be the thermal conductivity of graphene. The k_{g} of 2S is determined to be 359 W m^{-1} K^{-1}. Correspondingly, k_{m}, k_2 and k_3 are 0.40 W m^{-1} K^{-1}, 0.59 W m^{-1} K^{-1} and 0.78 W m^{-1} K^{-1} for 2S, respectively. Using the same method, k_{g} of 1S and 3S are determined to be 365 W m^{-1} K^{-1} and 273 W m^{-1} K^{-1}. Since the graphene layer distribution of sample 4S cannot be determined by the Raman method, k_{g} of 4S is calculated according to the following

equation: $k_{\mathrm{eff}} = (n_{\mathrm{a}}\delta k_{\mathrm{g}} + \delta_{\mathrm{p}} k_{\mathrm{p}})/(n_{\mathrm{a}}\delta + \delta_{\mathrm{p}})$. n_{a} is the average graphene layer number of 4S. k_{eff} of 4S is obtained as 0.38 W m^{-1} K^{-1}, and k_{g} is determined to be 33.5 W m^{-1} K^{-1} for sample 4S.

6. Results discussion

6.1. Variation of electrical and thermal conductivities among samples

Before we discuss the measured k_{g}, we would like to discuss the graphene quality of the four kinds of samples based on their electrical conductivity (σ) first, and then discuss how the σ and k_{g} vary among samples. Fig. 7(a) shows the σ and k_{g} variations with the graphene thickness δ_{g}. Due to the possible damage during the sample preparation process, the smallest σ of the four kinds of graphene samples is used, since these can best reflect the qualities of the graphene. The σ for 1S, 2S, 3S and 4S is determined to be 3.16×10^6 Ω^{-1} m^{-1}, 3.13×10^6 Ω^{-1} m^{-1}, 2.05×10^6 Ω^{-1} m^{-1} and 5.18×10^5 Ω^{-1} m^{-1}, respectively. The σ of 4S is about one-fifth of that for the other three. All these measured electrical conductivities are more than one order of magnitude lower than that of suspended graphene of high quality: 7×10^7 Ω^{-1} m^{-1}.[40] Also, it can be observed that k_{g} decreases with the increasing δ_{g}. The k_{g} of 4S is about one-ninth of that for the other three. The significantly reduced σ and k_{g} of 4S reflect the poor structure in 4S. Fig. 7(b) shows the correlated relationship between σ and k_{g}. The relationship of $\sigma \sim k_{\mathrm{g}}$ is quite linear, and the σ and k_{g} jointly reflect that the structure of the four samples becomes poorer with the increasing graphene thickness. To further investigate the poor structure of sample 4S, the Raman spectra of 4S is shown in Fig. 8 and will be discussed in detail later.

For 1S, 2S and 3S, the k_{g} at RT is a factor of ~8-fold lower than the reported value (3000 W m^{-1} K^{-1}) of suspended graphene.[2] This is understandable since their electrical conductivities are more than one order of magnitude lower than that of suspended graphene. The contribution to k from ZA mode
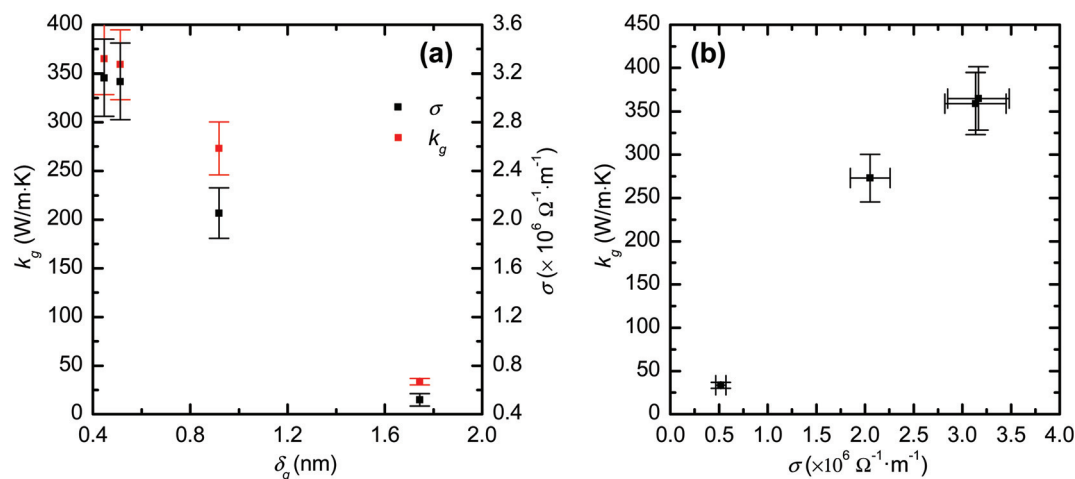

Fig. 7 (a) Variation of the thermal and electrical conductivities of graphene with its thickness. (b) Thermal conductivity of graphene variation against its electrical conductivity.
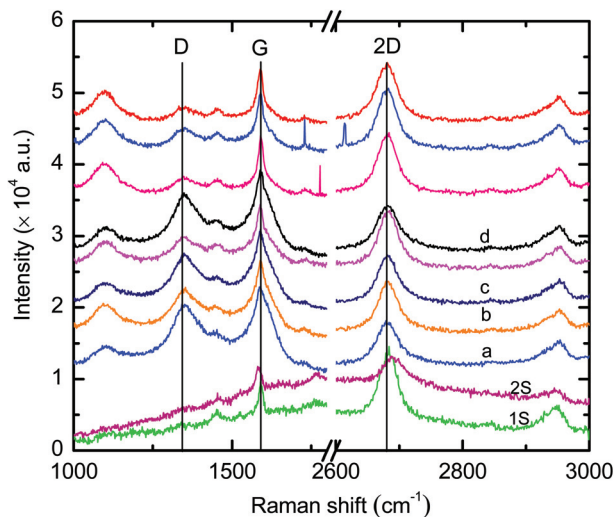
Fig. 8 Raman spectra of sample 4S. For comparison, spectra of 1S and 2S are also plotted in the figure. The Raman spectra of 4S exhibit three pronounced peaks at about 1346, 1589 and 2681 cm^{-1}, corresponding to the D band, G band and 2D band, respectively. No D band is observed from spectra of 1S and 2S. The existence of the D band in sample 4S indicates the disorder in the sp^2 domain. Both the D band and the G band of 4S are wide and overlap. This is the typical Raman spectrum of GO. It is speculated that there is GO in 4S. Besides, some G peaks of sample 4S (e.g., spectra a, b, c and d) show the characteristic of two peaks combination, which suggests the stratification among 5.2-layered graphene.

phonon scattering is significantly suppressed in supported graphene due to the phonon leakage across the interface between graphene and PMMA.[2,11,12] Our k_g of supported graphene is much smaller (~40% lower) than the k of supported graphene obtained by Seol et al.[11] (~600 W m^{-1} K^{-1}) and the value obtained by MD simulation (609 ± 19 W m^{-1} K^{-1}).[12] One fact needed to be pointed here is, in the k measurement and the simulation of above two references, the graphene is supported by SiO$_2$. In our experiment, the graphene is supported by PMMA. Ong et al. used the NEMD method to simulate the thermal transport in graphene sandwiched by SiO$_2$. When compared with supported graphene having weaker interface coupling strength (χ), the supported graphene with stronger χ has a larger k. It was suggested that the coupling of the graphene ZA modes to the substrate Rayleigh waves leads to enhancement in phonon velocity in supported graphene.[13] On the other hand, Chen et al. found that the increase of graphene–substrate coupling strength leads to shorter phonon lifetime and finally reduces the k.[12] We believe that besides the graphene–PMMA coupling strength, the atomic mass and the type of atom of the substrate also play an important role in affecting the thermal transport in graphene. There are abundant carbon atoms in PMMA. Under this situation, the ZA modes of graphene will be more easily coupled with PMMA (C atoms) than that between graphene and other substrates of heavier or lighter atoms. This ready momentum and energy coupling between C atoms in graphene and the C atoms in

PMMA will result in stronger scattering of phonons in graphene, leading to more thermal conductivity reduction. In Chen's work, they predicted the k of SiO$_2$-supported FLG with 52 Å width and 300 Å length by MD simulation. It is found that the k of FLG increases rapidly with the layer number and finally saturates at the level of graphite.[12] In our work, the k_g of FLG linearly decreases with the increasing average layer number of the four kinds of samples. This observation is rather related to the structure of the sample, not simply the layer number. From the difference between the Raman spectra of 1S, 2S and that of 4S (in Fig. 8), and the electrical conductivity difference among the four kinds of samples, it is concluded that there are different defect levels in the four graphene samples.

6.2. Structure study based on Raman spectroscopy

The k_g of our sample 4S is significantly lower than that of the other three graphene samples. Representative Raman spectra of 4S are shown in Fig. 8 in anticipation to explain the physics behind this significantly lower k_g. For comparison, the Raman spectra of 1S and 2S are also presented in the figure. A pronounced D band is observed in sample 4S while no D band is observed in both 1S and 2S. The D band is related to the breathing modes in the sp^2 carbon rings which are adjacent to the graphene edge.[22,41] Also, some G peaks of the Raman spectra (e.g., spectra a, b, c and d) show stratification among multiple-layered graphene of 4S. Taking spectrum a as an example, the G peak of spectrum a is asymmetrical, and the single peak Gaussian function could not fit it well. Two peak Gaussian function fits it well, indicating that there is stratification in sample 4S. Besides, from the Raman spectra a, b, c and d shown in Fig. 8, it can be seen that both the D band and the G band are wide and overlap. This is a typical Raman spectrum of graphene oxide (GO).[42] Based on these observations, we speculate the existence of GO in sample 4S. It is reasonable that sample 4S is a composite of graphene and GO. The in-plane k of the free-standing reduced GO film is reported to be ~61 W m^{-1} K^{-1}.[43] To conclude, we ascribe the lower k_g of 4S to the disorder defects in the sp^2 domain, the stratification among the multi-layered graphene and the existence of GO sheets. Besides, it is observed that there are peaks at ~1454 cm^{-1}, ~1732 cm^{-1} and ~2952 cm^{-1} from the 4S Raman spectra. They are the peaks of PMMA.[44] The peak at ~1096 cm^{-1} is not recognized and it may arise due to the background. These peaks have no effects on studies of graphene quality.

The Raman spectrum linewidth (Γ: cm^{-1}) provides a good way to estimate the phonon lifetime. Phonon scattering dominates the thermal transport in graphene. The optical phonon lifetime (τ) has the following relationship with Γ: $\tau^{-1} = 2\pi c\Gamma$, where c (3 × 10^{10} cm s^{-1}) is the speed of light.[45] Based on the Raman fitting of the four kinds of graphene samples, the linewidth of 4S (G peak) is ~50.2 cm^{-1}, which is much larger than the linewidth of 1S (~19.1 cm^{-1}), 2S (~18.9 cm^{-1}) and 3S (~16 cm^{-1}). According to the above equation, phonon scattering in the graphene of sample 4S has a much shorter phonon

lifetime. The optical phonon lifetime of sample 4S is estimated as 0.106 ps. This value is about one-tenth of the documented value of the optical phonon lifetime in SLG (1.2 ps).[46] Although this lifetime is only for the optical phonon probed in the Raman spectrum, it is expected the acoustic phonons in 4S graphene should have a similar order of lifetime shorter than that of phonons in the other graphene samples. As a result, the k_g of 4S is correspondingly much smaller than that of the other three kinds of supported graphene samples.

In graphene, phonons and electrons are the major energy carriers and phonons' contribution dominates.[47] So far, most of the experimental work measured the k of graphene using Raman spectroscopy. Recent numerical studies have posted a question about the non-equilibrium thermal state between phonons and electrons when the graphene is under laser irradiation during k measurement.[48] In the measurements based on optical heating, electrons are first heated in suspended graphene by electromagnetic excitation (light). Then the energy flows through electron–phonon (e–ph) scattering and phonon–phonon (ph–ph) scattering. Vallabhaneni *et al.* reported the temperature profiles of electrons, acoustic phonons and optical phonons in graphene based on BTE calculations. The laser power used in the simulation is 0.2 mW and the spot size is 0.25 μm. The average T of electrons is found to be the highest and the average T of optical phonons ranks second. The average T of acoustic phonons is the lowest. This means that during Raman spectroscopy measurement, the electrons and different mode phonons are not in thermal equilibrium. To be more specific, the ZA phonons have the largest non-equilibrium to other phonon modes. It is reported this would underestimate the k of graphene due to the fact that ZA phonons dominate the thermal transport.[48,49] In our differential technology to measure the k of supported graphene, this problem will not occur. Since the characteristic time of temperature rise is in the order of seconds and the sample is ∼mm long, it provides enough time and space for electrons and different phonons to reach thermal equilibrium during the measurement. The TET technique offers a quick and reliable method to measure the k of graphene while avoiding the thermal non-equilibrium problem among electrons, optical phonons and acoustic phonons.

ported graphene was determined around ∼0.1. Using our TET technique based on a differential treatment, the k_g of 1.33-layered, 1.53-layered, 2.74-layered and 5.2-layered supported graphene was measured to be 365 W m^{-1} K^{-1}, 359 W m^{-1} K^{-1}, 273 W m^{-1} K^{-1} and 33.5 W m^{-1} K^{-1}, respectively. These values are a factor of ∼8 lower than the reported k of suspended graphene (∼3000 W m^{-1} K^{-1}). This thermal conductivity reduction is attributed to suppressed ZA phonon contribution by the substrate, and the abundant C atoms in PMMA which are more easily coupled with graphene atoms than other substrates of heavier or lighter atoms. Our Raman spectroscopy study showed the existence of GO sheets, disorder in sp^2 domain and stratification in the 5.2-layered supported graphene. All these factors combined together and led to more k_g reduction in the 5.2-layered supported graphene. The electrical conductivity of sample 4S was determined to be 5.18 × 10^5 Ω^{-1} m^{-1}, which is only one-fifth of those of 1S (3.16 × 10^6 Ω^{-1} m^{-1}), 2S (3.13 × 10^6 Ω^{-1} m^{-1}) and 3S (2.05 × 10^6 Ω^{-1} m^{-1}). This, from another aspect, proved the poorer graphene quality in sample 4S. Our graphene size reached a level of ∼mm, far above the samples studied in the past. This giant graphene measurement significantly suppressed the thermal contact resistance problems and edge phonon scattering encountered in graphene k measurement at the μm scale. Since the characteristic time of temperature rise in our measurement is in the order of seconds and the sample is ∼mm long, electrons and different mode phonons could have sufficient time and space to reach thermal equilibrium during the measurement. The TET technique offers a quick and reliable method to measure the k of graphene while avoiding the thermal non-equilibrium problem among electrons, optical phonons and acoustic phonons.

Acknowledgements

7. Conclusion

In summary, first we reported the $R \sim T$ relationship for different-layered supported graphene since this relation is critical for explaining the graphene behavior in our thermal characterization. Our samples' dR/dT reduced from a positive value at RT to a negative value at low temperatures (∼10 K), while free-standing graphene has a negative value across the whole temperature range. This is due to the different thermal expansion coefficients of graphene and PMMA and the strain/stress built in graphene under temperature variation. During our thermal characterization, we also examined the surface emissivity precisely. The hemispherical emissivity of the sup-

References

1 K. S. Novoselov, A. K. Geim, S. V. Morozov, D. Jiang, Y. Zhang, S. V. Dubonos, I. V. Grigorieva and A. A. Firsov, *Science*, 2004, **306**, 666–669.

2 A. A. Balandin, S. Ghosh, W. Z. Bao, I. Calizo, D. Teweldebrhan, F. Miao and C. N. Lau, *Nano Lett.*, 2008, **8**, 902–907.

3 G. Q. Xin, T. K. Yao, H. T. Sun, S. M. Scott, D. L. Shao, G. K. Wang and J. Lian, *Science*, 2015, **349**, 1083–1087.

4 A. K. Geim and K. S. Novoselov, *Nat. Mater.*, 2007, **6**, 183–191.

5 F. Bonaccorso, Z. Sun, T. Hasan and A. C. Ferrari, *Nat. Photonics*, 2010, **4**, 611–622.

6 C. Lee, X. D. Wei, J. W. Kysar and J. Hone, *Science*, 2008, **321**, 385–388.

7 Q. Zhou, J. L. Zheng, S. Onishi, M. F. Crommie and A. K. Zettl, *Proc. Natl. Acad. Sci. U. S. A.*, 2015, **112**, 8942–8946.

8 S. S. Chen, Q. Z. Wu, C. Mishra, J. Y. Kang, H. J. Zhang, K. J. Cho, W. W. Cai, A. A. Balandin and R. S. Ruoff, *Nat. Mater.*, 2012, **11**, 203–207.

9 L. Lindsay, D. A. Broido and N. Mingo, *Phys. Rev. B: Condens. Matter*, 2011, **83**, 235428.

10 S. Ghosh, W. Z. Bao, D. L. Nika, S. Subrina, E. P. Pokatilov, C. N. Lau and A. A. Balandin, *Nat. Mater.*, 2010, **9**, 555–558.

11 J. H. Seol, I. Jo, A. L. Moore, L. Lindsay, Z. H. Aitken, M. T. Pettes, X. S. Li, Z. Yao, R. Huang, D. Broido, N. Mingo, R. S. Ruoff and L. Shi, *Science*, 2010, **328**, 213–216.

12 J. Chen, G. Zhang and B. W. Li, *Nanoscale*, 2013, **5**, 532–536.

13 Z. Y. Ong and E. Pop, *Phys. Rev. B: Condens. Matter*, 2011, **84**, 075471.

14 B. Qiu, Y. Wang, Q. Zhao and X. L. Ruan, *Appl. Phys. Lett.*, 2012, **100**, 233105.

15 X. F. Xu, L. F. C. Pereira, Y. Wang, J. Wu, K. W. Zhang, X. M. Zhao, S. Bae, C. T. Bui, R. G. Xie, J. T. L. Thong, B. H. Hong, K. P. Loh, D. Donadio, B. W. Li and B. Ozyilmaz, *Nat. Commun.*, 2014, **5**, 3689.

16 J. U. Lee, D. Yoon, H. Kim, S. W. Lee and H. Cheong, *Phys. Rev. B: Condens. Matter*, 2011, **83**, 081419(R).

17 Y. Wang, A. K. Vallabhaneni, B. Qiu and X. L. Ruan, *Nanoscale Microscale Thermophys. Eng.*, 2014, **18**, 155–182.

18 Z. Yan, J. Lin, Z. W. Peng, Z. Z. Sun, Y. Zhu, L. Li, C. S. Xiang, E. L. Samuel, C. Kittrell and J. M. Tour, *ACS Nano*, 2012, **6**, 9110–9117.

19 J. Guo, X. Wang and T. Wang, *J. Appl. Phys.*, 2007, **101**, 063537.

20 H. Lin, S. Xu, Y. Q. Zhang and X. W. Wang, *ACS Appl. Mater. Interfaces*, 2014, **6**, 11341–11347.

21 D. Graf, F. Molitor, K. Ensslin, C. Stampfer, A. Jungen, C. Hierold and L. Wirtz, *Nano Lett.*, 2007, **7**, 238–242.

22 S. Some, Y. Kim, Y. Yoon, H. Yoo, S. Lee, Y. Park and H. Lee, *Sci. Rep.*, 2013, **3**, 1929.

23 E. Ochoa-Martinez, M. Gabas, L. Barrutia, A. Pesquera, A. Centeno, S. Palanco, A. Zurutuza and C. Algora, *Nanoscale*, 2015, **7**, 1491–1500.

24 E. X. Perez, Ph.D. thesis, Universitat Rovira i Virgili, 2007.

25 R. J. Crawford, *Plastics Engineering*, Elsevier Butterworth-Heinemann, Oxford, 3rd edn, 1998, ch. 2, p. 59.

26 Y. S. Xie, Z. L. Xu, S. Xu, Z. Cheng, N. Hashemi, C. Deng and X. W. Wang, *Nanoscale*, 2015, **7**, 10101–10110.

27 J. H. Hinnefeld, S. T. Gill, S. Zhu, W. J. Swanson, T. Li and N. Mason, *Phys. Rev. Appl.*, 2015, **3**, 014010.

28 M. Esposito, S. Buontempo, A. Petriccione, M. Zarrelli, G. Breglio, A. Saccomanno, Z. Szillasi, A. Makovec, A. Cusano, A. Chiuchiolo, M. Bajko and M. Giordano, *Sens. Actuators, A*, 2013, **189**, 195–203.

29 D. Yoon, Y. W. Son and H. Cheong, *Nano Lett.*, 2011, **11**, 3227–3231.

30 N. Mounet and N. Marzari, *Phys. Rev. B: Condens. Matter*, 2005, **71**, 205214.

31 W. Z. Bao, F. Miao, Z. Chen, H. Zhang, W. Y. Jang, C. Dames and C. N. Lau, *Nat. Nanotechnol.*, 2009, **4**, 562–566.

32 H. Lin, S. Xu, X. W. Wang and N. Mei, *Small*, 2013, **9**, 2585–2594.

33 G. Q. Liu, S. Xu, T. T. Cao, H. Lin, X. D. Tang, Y. Q. Zhang and X. W. Wang, *Biopolymers*, 2014, **101**, 1029–1037.

34 K. F. Mak, M. Y. Sfeir, Y. Wu, C. H. Lui, J. A. Misewich and T. F. Heinz, *Phys. Rev. Lett.*, 2008, **101**, 196405.

35 R. R. Nair, P. Blake, A. N. Grigorenko, K. S. Novoselov, T. J. Booth, T. Stauber, N. M. R. Peres and A. K. Geim, *Science*, 2008, **320**, 1308–1308.

36 J. M. Dawlaty, S. Shivaraman, J. Strait, P. George, M. Chandrashekhar, F. Rana, M. G. Spencer, D. Veksler and Y. Q. Chen, *Appl. Phys. Lett.*, 2008, **93**, 131905.

37 A. Soldera and J. P. Dognon, *Macromol. Symp.*, 1997, **119**, 157–164.

38 W. W. Cai, A. L. Moore, Y. W. Zhu, X. S. Li, S. S. Chen, L. Shi and R. S. Ruoff, *Nano Lett.*, 2010, **10**, 1645–1651.

39 E. H. Weber, B.S. thesis, Michigan Technological University, 2001.

40 X. Y. Fang, X. X. Yu, H. M. Zheng, H. B. Jin, L. Wang and M. S. Cao, *Phys. Lett. A*, 2015, **379**, 2245–2251.

41 A. C. Ferrari, *Solid State Commun.*, 2007, **143**, 47–57.

42 K. N. Kudin, B. Ozbas, H. C. Schniepp, R. K. Prud'homme, I. A. Aksay and R. Car, *Nano Lett.*, 2008, **8**, 36–41.

43 J. D. Renteria, S. Ramirez, H. Malekpour, B. Alonso, A. Centeno, A. Zurutuza, A. I. Cocemasov, D. L. Nika and A. A. Balandin, *Adv. Funct. Mater.*, 2015, **25**, 4664–4672.

44 R. Cusco, E. Alarcon-Llado, J. Ibanez, L. Artus, J. Jimenez, B. G. Wang and M. J. Callahan, *Phys. Rev. B: Condens. Matter*, 2007, **75**, 165202.

45 K. J. Thomas, M. Sheeba, V. P. N. Nampoori, C. P. G. Vallabhan and P. Radhakrishnan, *J. Opt. A: Pure Appl. Opt.*, 2008, **10**, 055303.

46 K. Kang, D. Abdula, D. G. Cahill and M. Shim, *Phys. Rev. B: Condens. Matter*, 2010, **81**, 165405.

47 D. L. Nika and A. A. Balandin, *J. Phys.: Condens. Matter*, 2012, **24**, 233203.

48 A. K. Vallabhaneni, J. Loy, D. Singh, X. L. Ruan and J. Murthy, *Proceedings of the ASME 2013 International Mechanical Engineering Congress and Exposition, San Diego*, 2013.

49 P. Virtanen, *Phys. Rev. B: Condens. Matter*, 2014, **89**, 245409.